Aerodynamic Performance of Micro Aerial Wing Structures at Low Reynolds Number

Y. D. DWIVEDI*,[1], Vasishta BHARGAVA[2], P. M. V. RAO[3], Donepudi JAGADEESH[4]

*Corresponding author
*,[1]Institute of Aeronautical Engineering,
Dundigal, Hyderabad500043, Telangana, India,
yddwivedi@gmail.com
[2]Sreyas Institute of Engineering & Technology,
Hyderabad500068, India,
vasishtab@gmail.com
[3]Vignan University,
Vaddeshwaram, Guntur, Andhra Pradesh, India
[4]Narasaraopeta Engineering College,
Narasaraopet, Andhra Pradesh 522601, India,
jagadish.donepudi@gmail.com

DOI: 10.13111/2066-8201.2019.11.1.8

Received:19 December 2018/ Accepted: 20 February 2019/ Published: March 2019

Abstract: *Corrugations are folds on a surface as found on wings of dragon fly insects. Although they fly at relatively lower altitudes its wings are adapted for better aerodynamic and aero-elastic characteristics. In the present work, three airfoil geometries were studied using the 2-D panel method to evaluate the aerodynamic performance for low Reynolds number. The experiments were conducted in wind tunnel for incompressible flow regime to demonstrate the coefficients of lift drag and glide ratio at two Reynolds numbers $1.9x10^4$ and $1.5x10^5$ and for angles of attack ranging between 0^0 and 16^0. The panel method results have been validated using the current and existing experiment data as well as with the computational work from cited literature. A good agreement between the experimental and the panel methods were found for low angles of attack. The results showed that till 8^0 angle of attack higher lift coefficient and lower drag coefficient are obtainable for corrugated airfoils as compared to NACA 0010. The validation of surface pressure coefficients for all three airfoils using the panel method at 4^0 angles of attack was done. The contours of the non-dimensional pressure and velocity are illustrated from -10^0 to 20^0 angles of attack. A good correlation between the experiment data and the computational methods revealed that the corrugated airfoils exhibit better aerodynamic performance than NACA 0010.*

Key Words: *Corrugated airfoil, Lift coefficient, Drag coefficient, Panel method, Reynolds number*

1. INTRODUCTION

The nature gives effective, robust and straightforward solutions for engineering problems and this practice is becoming very popular day by day [21]. The profound understanding of nature and of its way to overcoming the problem of flight in natural avian like birds and insects has led to tremendous improvements in the aerodynamics of manmade aerial

vehicles. Creatures of flight, such as birds and insects have inspired human to design aircrafts of various types and sizes. Specifically, the smooth airfoil shapes of familiar aircrafts are inspired by the birds' wing [16]. The smaller aircrafts like unmanned aerial vehicles (UAVs) operate at significantly lower Reynolds number, where the performance of the conventional airfoils is no longer better [2]. The aerodynamic effects of low Reynolds numbers on corrugated wings were studied by several researchers [5], [6], [11], [12], [17]. It was found that most insects' wings specifically dragonflies and locusts have high agility and maneuverability. These insects are competent to hover, climb, dive, land and take-off at different wind speeds and ambient conditions. Another investigation reported that the remarkable aerodynamic performance of dragonfly's wings was caused by the muscular morphing and wing geometry, specially the wing corrugation [4]. Extensive biological and aerodynamic study has been carried out by many researchers to demonstrate the reasons for the superior flight by flapping motion of the wings and the corrugated wing airfoil [28].They revealed that the flapping produces significant lift by generating low pressure leading edge vortex (LEV) while corrugated cross section, reduces the overall flow separations in both flapping and static motion. The effects of corrugations were demonstrated, and the results are reported in several experimental studies such as [10], [19]. These reports confirmed that the corrugation initiates an early transition to turbulent flow thus reducing separation and delay in stall. A better aerodynamic characteristic obtained using pleated airfoil at first sight seems to contradict with the idea of streamlined airfoils used in conventional aircrafts. However recent studies [14], [15], [27], [29] suggested otherwise. There also have been several studies related to aerodynamic forces which were conducted on actual dragonflies and dragonfly's modeled airfoils to measure the forces associated with both flapping and gliding modes of operation. Some of the more notable and recent studies for gliding flight of a dragonfly's wing are the numerical and experimental studies conducted by [8], [13], [23], [25, 26], [30]. More recently [3], [7], [22] have performed 3-D computational study on different types of corrugated wings by using commercially available computational software. However, these studies have been primarily conducted at chord Reynolds number 10^4 or less, which is considerably lower than the range used for micro aerial vehicles (MAVs). The aim of the present work is to analyze two different types of corrugation in relation to the coefficients of lift, drag and glide ratio, which are also relevant for MAVs. To the best of our knowledge no studies have been conducted before on bio-inspired corrugated wing using the panel method. The other aim is to explore whether the 2-D panel method can predict low Reynolds number flows fairly accurately and agree with experiment data conducted on similar airfoils.

2. METHODOLOGY

2.1 Numerical Formulation

Panel methods are designed for potential flows which are commonly used in analysis of 2D lifting flows that have negligible or low viscosity. For computational analysis, it is known that velocity potential function can be readily used to describe the aerodynamic flow field around the arbitrary shaped body than streamline function. This is because for both the2D and 3D analysis of flow, the velocity field exists at every coordinate on the surface; however for the stream function the derivatives of velocity vector becomes complex for the analysis of the3D flow. The basic approach involved in panel methods is a combination of source and sink which have equal strength, *K*, presented in a uniform distributed flow pattern around an arbitrary body. The source strengths are defined in such a way that appears in the fluid field as streamlines at a uniform rate while sink disappears at a same rate [9], [18]. For any given

arbitrary shaped body, the geometry is divided into a specific number of panels representing the surface. The panels represent the approximation of the geometry surface, using straight line segments. For a given AOA, α, the steps involved are as follows:

1. Number the panels, sequentially from 1 … X,
2. Calculate the center point also known as collocation or control point for defined panels representing the geometry,
3. Most appropriate boundary condition for airfoil airfoils, using panel method involves impermeable flow perpendicular to the surface describing the airfoil,
4. A set of unit vectors are applied in a perpendicular and tangential directions, N_{ij} and $T_{ij,}$
5. Velocity field is derived by taking into account any of the two panels, *I & j*, source strength of individual panel *j* induced on panel *i* with respect to streamwise direction,
6. After defining the local velocity vector for all the panels of the discretized airfoil surface, the influence coefficients are evaluated for each panel in perpendicular and tangential directions, respectively,
7. Unknown source and vortex strengths, σ, γ are evaluated for each panel,
8. Finally, the tangential velocity vector field over the airfoil surface is calculated using the known values of influence coefficients on every panel i.e. the normal (C_n) and tangential (C_t) directions, represented by matrix, M, source and vortex strength, matrix A and vertical velocity components on each panels, matrix B. The tangential velocity vector is used to determine the surface pressure coefficient along the chord length of the airfoil surface.

It must be noted that in MATLAB for all the variables i.e. velocity and its components, matrices are essential and required to solve the system of discrete equations. The surface pressure coefficient can be expressed using the Eq. (1). Another boundary condition also known as *"Kutta condition"* is imposed on trailing edge panels to account for the flow near the trailing edge so that tangential velocity vector for trailing edge panels equals in magnitude on upper and lower surfaces of airfoil [1], [9]. The surfaces represented by the panels are typically solid rectangular or curvilinear areas upon which the above conditions are applied. Therefore, *X+1* system of linear algebraic equations is solved for *X*+1 unknown source strengths, σ_i, using the influence coefficients and written in matrix form as shown in the flow chart for computational routine in Fig. 1. The pressure acting at any collocation point *i* on the panel surface can be expressed in anon-dimensional form as in Eq. (1)

$$C_{p_i} = 1 - \left[\frac{V_{t_i,}}{U}\right]^2 \tag{1}$$

The number of panel nodes used in the simulation depends on smoothness or fineness of corrugations on the surface and the maximum panel angle for trailing edge is 90^0. The lift and drag coefficient for the standard airfoil specimens by [24] can be found using Eq. (2) & Eq. (3)

$$C_L = L/(0.5\rho U^2 S) \tag{2}$$

$$C_D = D/(0.5\rho U^2 S) \tag{3}$$

Where ρ is the fluid density, *U* is the free stream velocity and *S* is the planform area, the coefficients of total lift are denoted by C_L and the total drag is denoted by C_D. They are obtained using the pressure coefficient between the upper and the lower surfaces for each panel, multiplied with its panel length and integrating them at any given angle of attack. Further, the lift and drag coefficients could also be evaluated using the normal and tangential force influence coefficients as given by Eq. (4) and Eq. (5)

$$C_L = C_n \cdot \cos\alpha - C_t \cdot \sin\alpha \quad (4)$$

$$C_D = C_n \cdot \sin\alpha + C_t \cdot \cos\alpha \quad (5)$$

Aerodynamic performance of a wing during gliding can therefore be determined by Eq. (6)

$$\epsilon_R = C_L/C_D \quad (6)$$

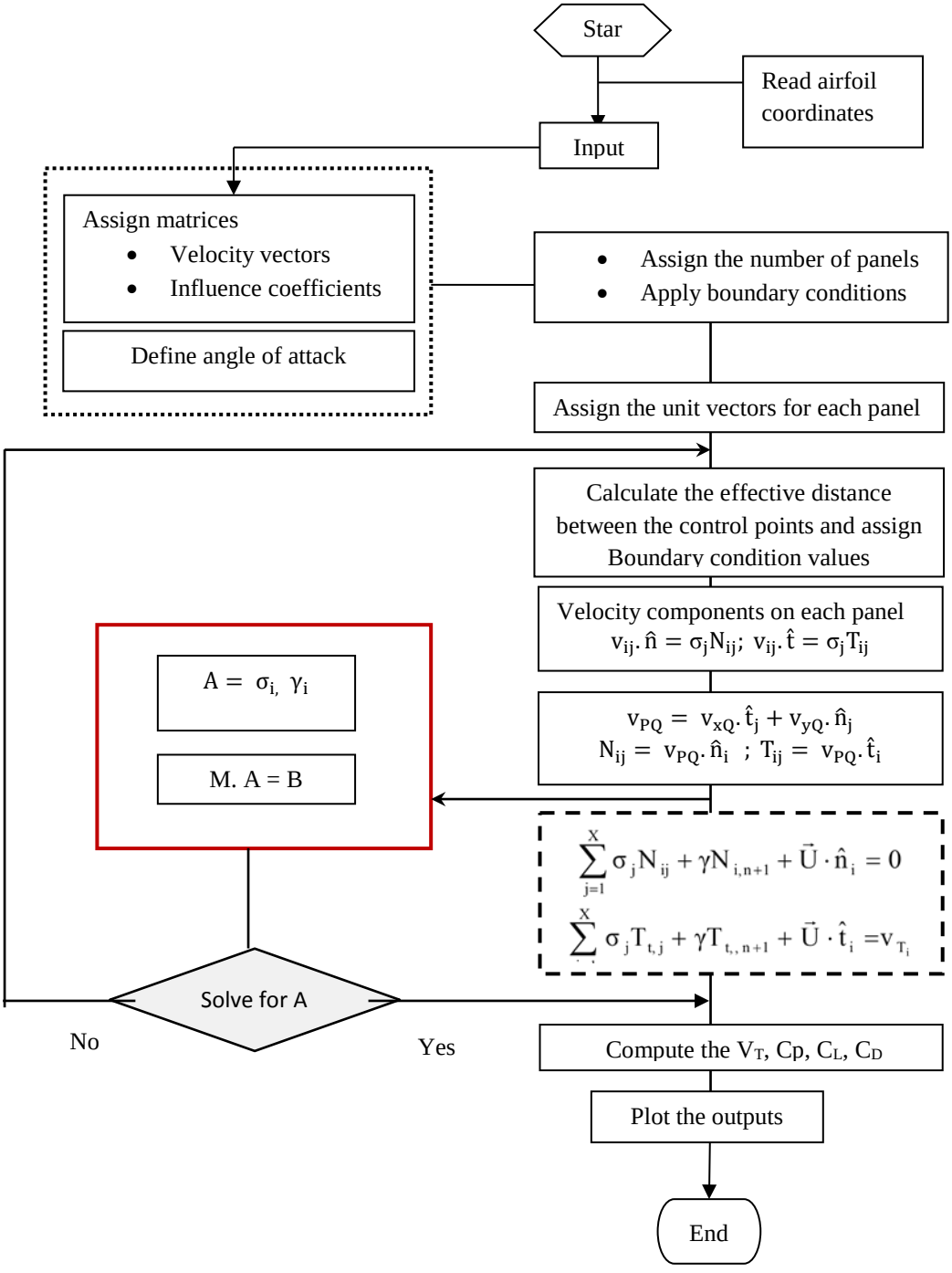

Figure 1. Flow chart of computational routine implemented in MATLAB

2.2 Geometry of airfoils

The geometries of corrugated airfoils were selected based upon the previous experimental and numerical investigations [11] [19] [28] and shown in Table 1. It can be seen from the Figure 2(a), for corrugated A airfoil; the corrugations are observed throughout its chord length. For corrugated B airfoil, sharp peaks are presented near the leading edge up to 30 % of the chord length followed by a broad hump present towards the trailing edge as shown in Fig. 2 (b). The corrugated airfoil used by Kessel, Murphy and Hu resembles the shape of corrugated A airfoil used in the present study, at the leading edge, and up to ~ 50 % of the chord length while the airfoil used by [7] resembles closely to the corrugated B airfoil. It is also identical to the airfoil 2 used by Kessel in his investigation. These similarities in airfoils enable better validation of results with those obtained from the earlier computational investigations [28].

Table 1. Dimensions for NACA 0010, Corrugated A and Corrugated B airfoil

Airfoil	Chord [m]	Max. thickness [m]	Thickness/ chord ratio [%]
NACA 0010	0.12	0.012	10
Corrugated A	0.12	0.006	5.0
Corrugated B	0.12	0.008	6.6

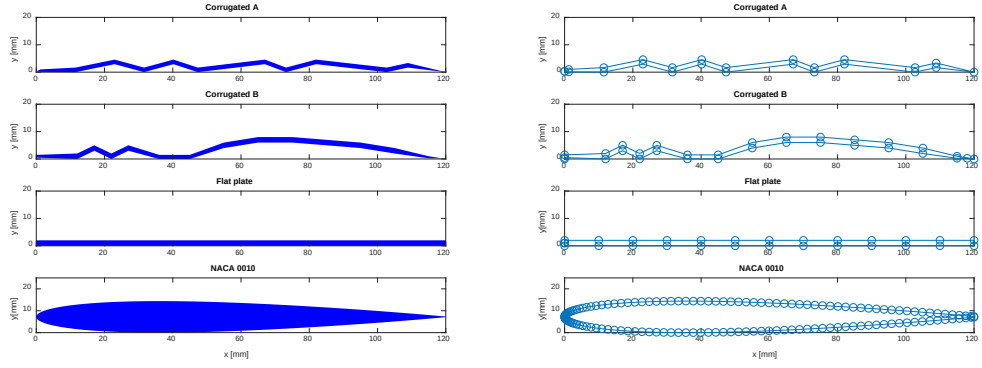

Figure 2. (a) Geometry of Corrugated A, Corrugated B, Flat plate and NACA 0010, (b) panel approximation

2.3 Experimental setup

The low speed subsonic open circuit wind tunnel facility was used for the present experimental work. It has three main sections, an inlet section, the nozzle and the test section and a diffuser section at the exit of the tunnel. The dimensions of the sections and the corresponding principal functions are shown in Table 2. Schematic representation of the open circuit wind tunnel test section used for experiments is shown in Fig. 3 (a). The smoke rake provided in contraction cone just before the test section is used to view the smoke flow. The velocity and pressure distribution can be measured by the inclined tube manometer as shown in Fig. 3(b). The two limbs of the manometer are connected to the static pressure holes, one in the settling chamber just before the contraction side and the other to the start of the test section.

The reading in the manometer shows the dynamic head of the fluid in the test section and it serves as the reference for keeping the tunnel speed constant. The inclination of the manometer is kept at 30^0 to the horizontal, at this angle the liquid column length change is twice to the vertical head, to provide better accuracy. The tunnel is also provided with a Pitot static tube, which can be traversed across the tunnel section. The fan is connected with

variable speed motor, which is varied by the AC controller and the motor required 3 phase A.C power which is equipped with six component force balance, pressure distribution system, and manometer. The snapshot of full experimental setup is shown in Fig. 4(a) and the fabricated corrugated A airfoil in wind tunnel is shown in Fig. 4(b).

Table 2. Wind tunnel specifications

Nozzle / test section	Value	Description
Contraction ratio	9:1	Used to increase speed of incoming air flow
Contraction length	1.8m	Distance over which air speed is incremented
Stainless screens	8 x 16 grid	Intended to reduce turbulence in test section
Test section	0.6m x 0.6m x 2m	Space to install model test specimen
Max wind speed	50 m/s	Design speed of wind tunnel
Diffusor section		
Axial flow fan Diameter RPM No of Blades	 1.3m 1450 12	To produce potential flow inside the tunnel at given free stream condition
Fan duct diameter	~ 1.4m	Diverging at the exit, with blade clearance,
Motor and stand	~ 20kW	Space to provide mounting and power axial fan
Diffusor /Transition		Reduces wind velocity
Inlet section		
Settling chamber	1.8m x 1.8m	Constant air flow stream ahead of contraction
Honey comb size	0.025m x0.025mx0.2m	Filter particulate matter from air flow stream

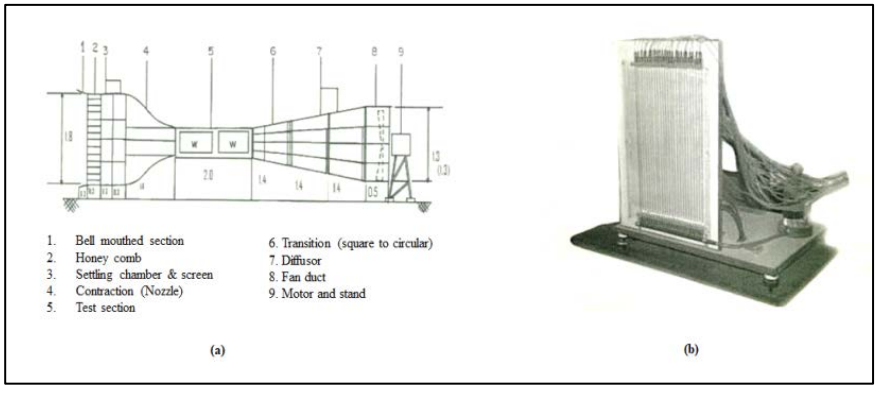

Figure 3. (a) Schematic diagram of wind tunnel; (b) Inclined tube manometer

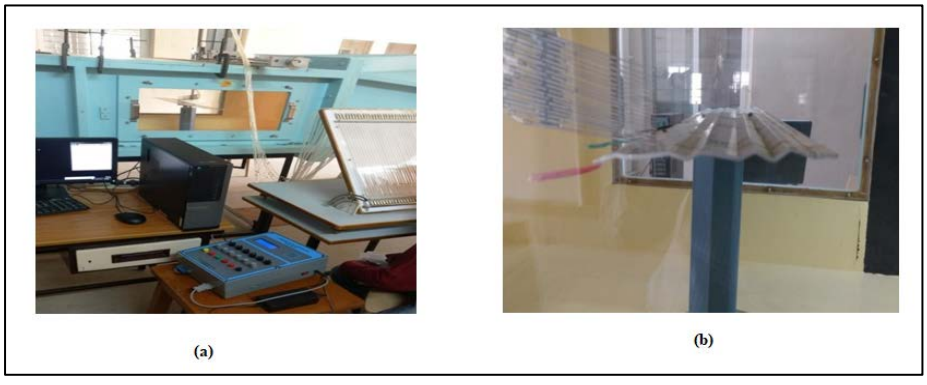

Figure 4. (a)Snapshot of experimental setup; (b) Corrugated A airfoil in wind tunnel

3. RESULTS AND DISCUSSIONS

3.1 Pressure coefficient distribution

A comparison of the pressure coefficients for upper and lower surfaces of NACA 0010, Corrugated A and Corrugated B airfoils are obtained using the panel method along the chord length for 4^0 angles of attack (AOA) and for Re ~19000. At 10% of the chord length from the leading edge, the difference in pressure coefficient between upper and lower surfaces is maximum, which in turn causes high lift coefficient. The pressure coefficient for NACA 0010 airfoil is found to decrease smoothly and for both the corrugated airfoils the pressure distribution is in zig-zag pattern along the chord near the sharp edges of the corrugations. Beyond 40% of the chord length the pressure coefficient rises up in Corrugated A and corrugated B airfoils, in comparison to NACA 0010 airfoil due to the presence of corrugations in the Corrugated A and hump in the Corrugated B airfoils as shown in Fig. 5(a). It is also observed from Fig. 5(b) that the pressure coefficient for the flat plate is smooth without any zig-zag along its chord length. For Corrugated A and Corrugated B airfoils, the effect of corrugations is seen as pressure peaks due to rapid fluctuations in the velocity distribution. The contours for the pressure coefficient for three airfoils are shown in Fig. 6(a) Fig. 6(b) and Fig. 6(c). It is observed that the pressure coefficient tends to rise with positive AOA. However, for the negative AOA, fluctuations are observed near the corrugated surfaces. However, for NACA 0010 airfoil smooth contours are seen along the chord length and resemble a symmetric pattern.

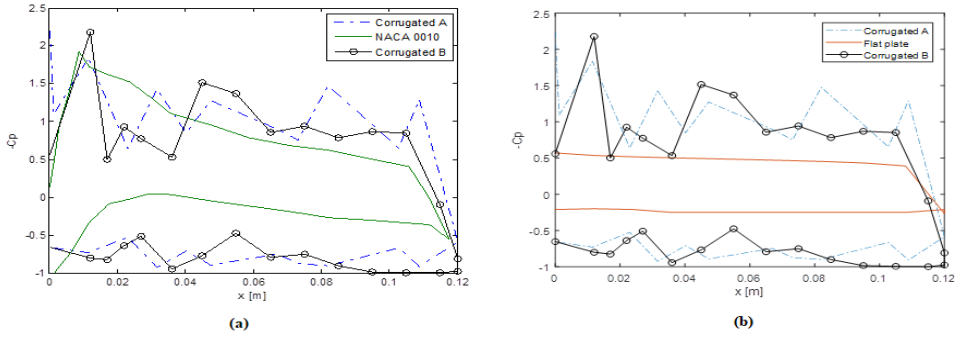

Figure 5. (a) Pressure coefficient distribution of NACA0010, Corrugated A and Corrugated B airfoils (b) Corrugated A, Corrugated B and flat plate using the2D panel method at 4^0 AOA at Re ~ 19000

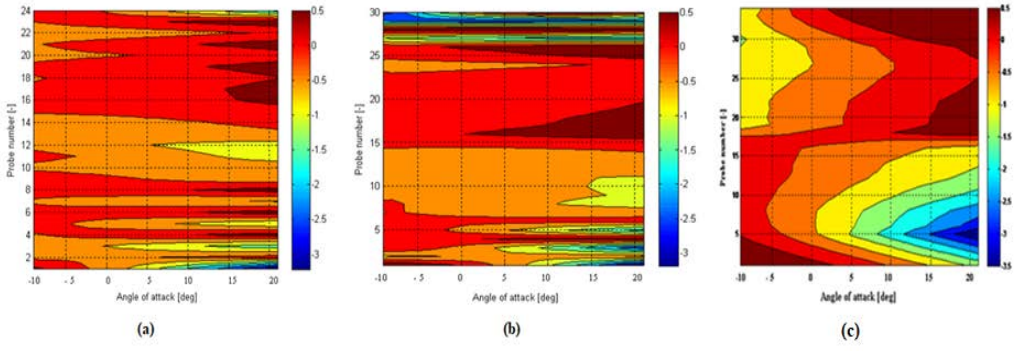

Figure 6. Pressure coefficient distribution of (a) Corrugated A, (b) Corrugated B (c) NACA 0010 Probe 1-14, upper surface & probe 15-27 lower surface of corrugated A, Probe 1-15, Upper surface & probe 16-31, Lower surface of corrugated B airfoil, at different AOA, -10^0 to 20^0

At 20% of the chord length, for both corrugated airfoils the velocity increased nearly 40 % for positive AOA.

However, for negative AOA it is found to be less than free stream value of 20 m/s. At 40 % of the chord length, the velocity is found to decrease in similar trend. Since NACA 0010 is a smooth and symmetric airfoil, there was no decrease in tangential velocity observed at 40 % of the chord length.

The pressure distribution also revealed that as the AOA increases the pressure coefficient also increases on the upper surface near the corrugation peaks. The trend is the same for all angles of attack, from -10^0 to 20^0 because of the symmetry in geometry. In contrast, the pressure coefficient contours for both corrugated airfoils obtained using the panel method on the lower surface is less prominent due to the decrease in the velocity gradient between the corrugations. Further for corrugated B airfoil they appear smooth but showed similar trends with corrugated A due to corrugations near the leading edge and broad hump near the trailing edge. The pressure distribution also revealed that as the angle of attack increases the pressure coefficient is increasing on the upper surface near the corrugation peaks which is seen for both A and B airfoils. For a given Reynolds number, the forces acting on airfoil surfaces are directly related to the pressure difference between the upper and lower surfaces:

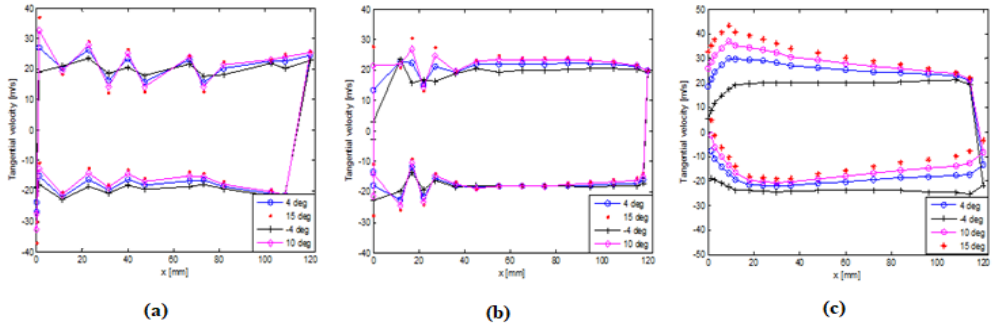

Figure 7. Tangential velocity distribution along chord; (a) for Corrugated A; (b) Corrugated B; (c) NACA 0010 airfoils at -4^0, 4^0, 10^0 and 15^0angle of attack for Re ~ 1.5 x10^5

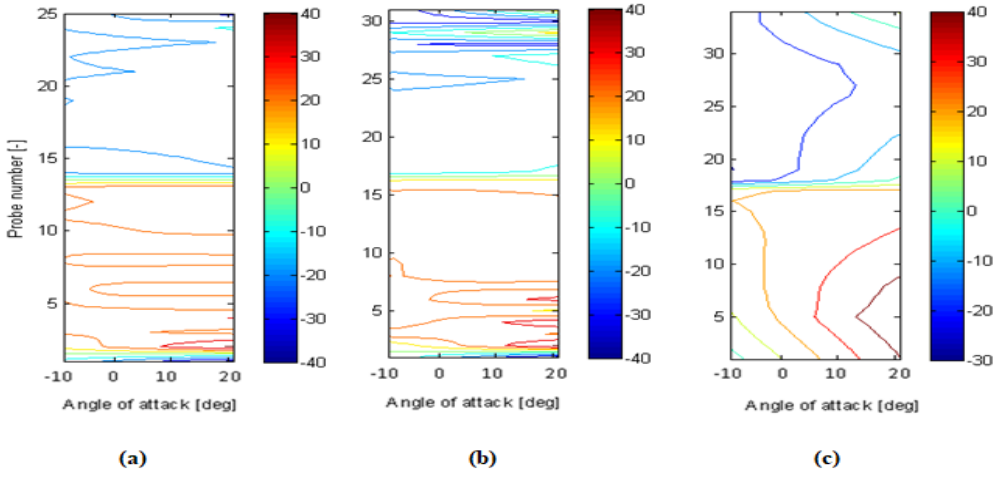

Figure 8. Velocity contours of; (a) corrugated A; (b) corrugated B; (c) NACA 0010 airfoils. Probe 1-14,Upper surface & probe 15-27, Lower surface of Corrugated A, Probe 1-15, Upper surface & probe 16-31, Lower surface of Corrugated B, Probe 1-17, Upper surface & probe 18-35 of the NACA 0010

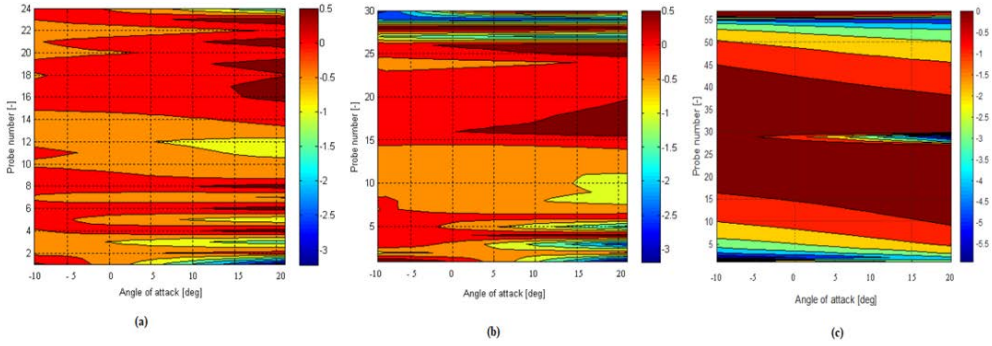

Figure 9. Pressure coefficient distribution of (a) Corrugated A; (b) Corrugated B; (c) Flat plate, Probe 1-14, upper surface & probe 15-27 lower surface of corrugated A, Probe 1-15, Upper surface & probe 16-31, Lower surface of corrugated B airfoil, at different angles of attack, -10^0 to 20^0

Further, from Fig. 7(a) and Fig. 7(b) the tangential velocity distribution on the surface of both corrugated airfoils showed abrupt variations near the corrugations. For the NACA 0010 and the flat plate, smooth variation in tangential velocity is observed as depicted in Fig. 7(c). From Fig. 8(a) and Fig. 8(b), the velocity contours for corrugated airfoils and the fluctuations in velocity are seen near the corrugated peaks whereas for NACA0010 airfoil a symmetric pattern with a continuous increase of velocity near the leading edge is observed with increasing AOA i.e. from -4^0 to 15^0 Figures 9(a) to Fig. 9(c) represent the contours of pressure coefficient for corrugated airfoils and compared with flat plate. Similarly, Fig. 10(a) to Fig. 10(c), Fig. 11 (a) to Fig. 11(c) show the tangential velocity distribution and velocity contours of the same airfoils, respectively.

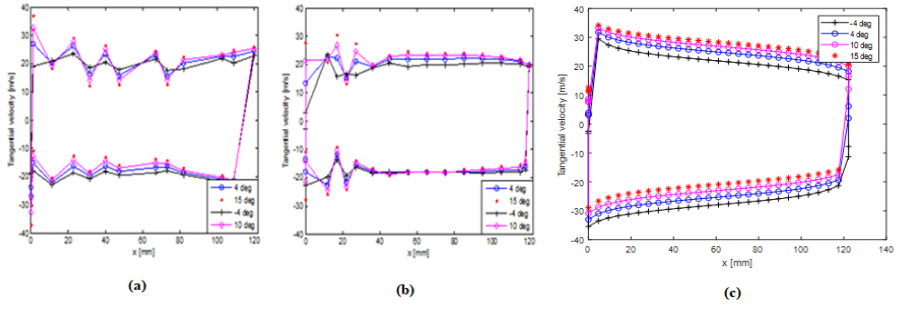

Figure 10. Tangential velocity distribution of (a) Corrugated A; (b) Corrugated B; (c) Flat plate, Probe 1-14, upper surface & probe 15-27 lower surface of corrugated A, Probe 1-15, Upper surface & probe 16-31, Lower surface of corrugated B airfoil, at -4, 4, 10 and 15 degrees angle of attack

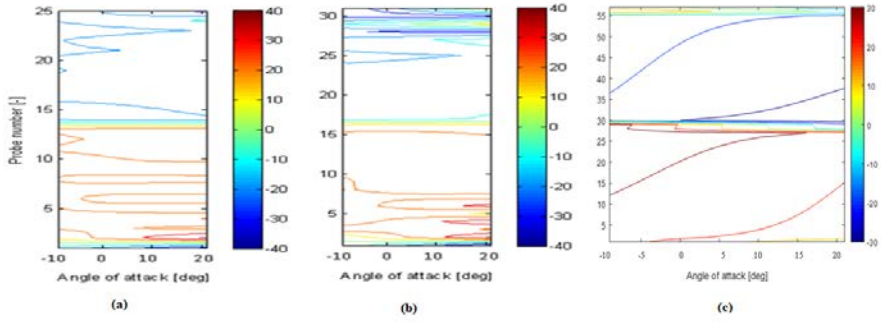

Figure 11. Velocity contours of (a) corrugated A (b) corrugated B (c) Flat plate airfoils. Probe 1-14,Upper surface & probe 15-27, Lower surface of Corrugated A, Probe 1-15, Upper surface & probe 16-31, Lower surface of Corrugated B

3.2 Effect of angle of attack on aerodynamic force coefficients

Fig. 12(a) and Fig. 12(b) shows the coefficient of lift and drag verses Angle of attack for NACA 0010, corrugated A and corrugated B using the panel method and *was evaluated between 0^0 and 16^0 angles of attack.*

The coefficient of lift for both the corrugated airfoils was found to be higher than the NACA0010.

Despite few corrugations than corrugated A airfoil, corrugated B airfoil showed higher lift for all angles of attack than the other two airfoils.

Until 8^0 angles of attack, the trends for lift coefficient for all airfoils are similar and arefound to vary almost linearly.

Also, the drag coefficient for both corrugated A and corrugated B airfoils were found to increase greater than the NACA 0010 airfoil for the angles of attack greater than 8^0. It must be noted that the increase in drag coefficient for both corrugated airfoils above 12^0 angles of attack is due to the flow separation from the suction side of airfoils surface at higher angles of attack.

In addition, the trends for drag coefficient for corrugated A and corrugated B airfoils was similar up to 12^0 angles of attack. Beyond this, rapid increase in drag coefficient of corrugated A is observed due to flow separation which is not found in corrugated B due to presence of hump near the trailing edge which reattaches the flow.

In the Figures 13(a) and Fig. 13(b) the experiment data for lift and drag coefficients for corrugated A and corrugated B airfoils are compared with results from the panel method and from (Ho & New, 2016).

The glide ratio shown in Fig. 14 (a) and Fig. 14 (b), Fig. 15(a) and Fig. 15 (b) for corrugated A, corrugated B airfoils were found to be high at 5^0angles of attack.

It is ~ 3% more than the corrugated B airfoil but found to deviate significantly with NACA 0010 by > 10%.

This trend continued till 5^0 angles of attack and for $\alpha > 8^0$ the glide ratio curve resembled the NACA 0010 airfoil.

The glide ratio for NACA 0010 was found higher than both the corrugated airfoils above 8^0 angles of attack due to smooth surface of NACA airfoil which helps in flow re-attachment. Thus, the glide ratio of corrugated airfoils is found relatively better than the NACA 0010 airfoil at low positive angles of attack ($<8^0$) for a given Reynolds number.

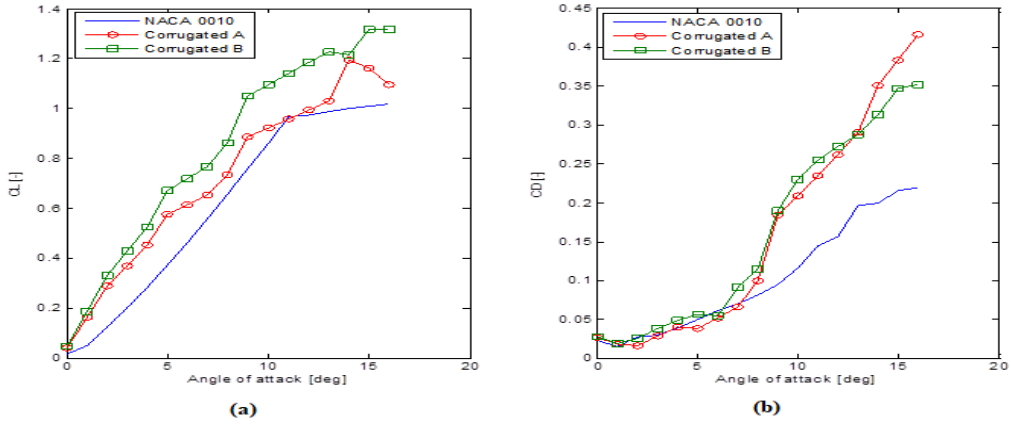

Figure 12. Results for NACA 0010, Corrugated A and Corrugated B airfoils by panel method between 0^0 and 16^0 angle of attack for Re ~19000 (a) lift (b) drag

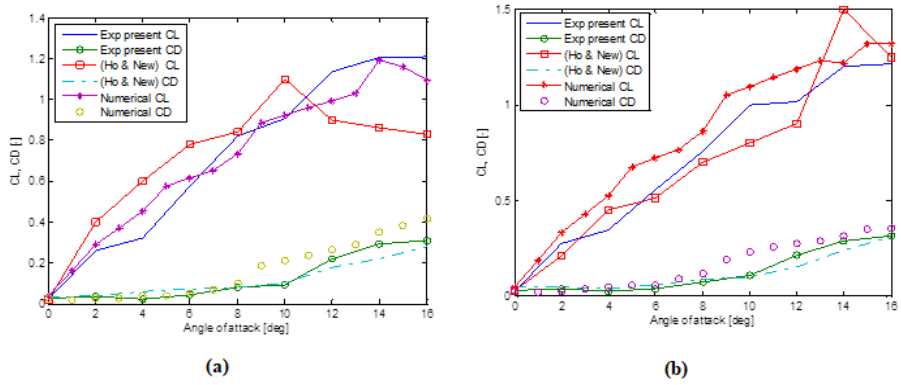

Figure 13. Comparison of lift and drag coefficient results by panel method (Re ~19000), Ho and New (2016) (Re-14000) and present experimental work between 0^0 -16^0 angles of attack (a) Corrugated A; (b) Corrugated B

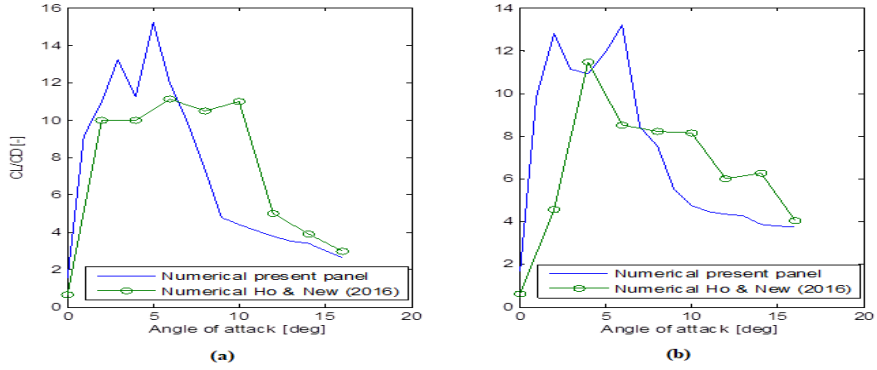

Figure 14. Comparisons of C_L/C_D by present panel method at Re~19000, Ho and New (2016) for Re – 14000, between 0^0 and 16^0 angles of attack. (a) Corrugated A; (b) Corrugated B

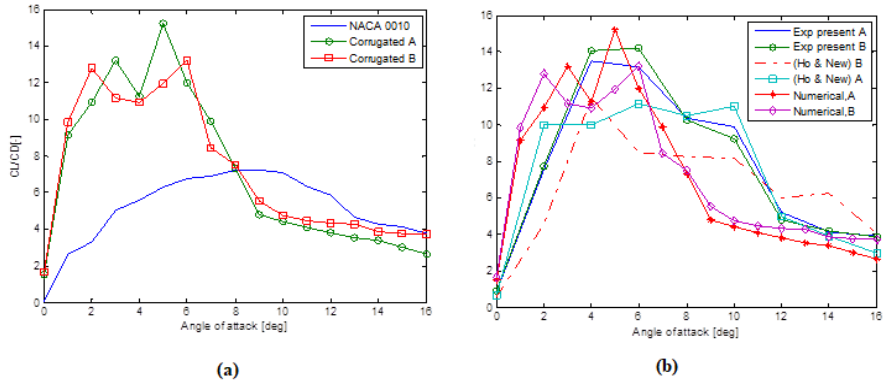

Figure15. (a) Comparison of C_L/C_D for NACA 0010, Corrugated A, and Corrugated B airfoils using panel method; (b) with panel method, Ho and New (2016) results and experiment data

3.3 Effect of number of panels on pressure coefficient distribution

As discussed in section 2.1, the 2D panel method approximates the geometric surface of airfoil into finite no of segments and evaluates the aerodynamic properties. Further to demonstrate the effect of number of panels on pressure distribution, a numerical experiment was conducted to test the change in the pressure peaks near corrugations along the chord

length. To do this, corrugated A airfoil was chosen and program was repeated using 25, 27, 31, 34 and 62 no of panels.

The boundary conditions were kept constant and for constant flow conditions i.e. Re -19000. It can be observed that with increase in no of panels the pressure coefficient approximation accuracy had increased by 1 % near corrugated peaks but a remarkable increase of 10% near troughs. This shows the effect of *panel leakage* caused due to discretization of airfoils surface results in numerical flow discontinuities or gaps at the node points for each panel along the chord length of airfoil.

This sort of numerical flow discontinuities is termed as *panel leakage* and reduced by considering more no of panels for a given geometry and improve the pressure coefficient approximation. Fig 16 illustrates the influence of no of panels for tested corrugated A airfoil surface evaluated at 2^0 angle of attack

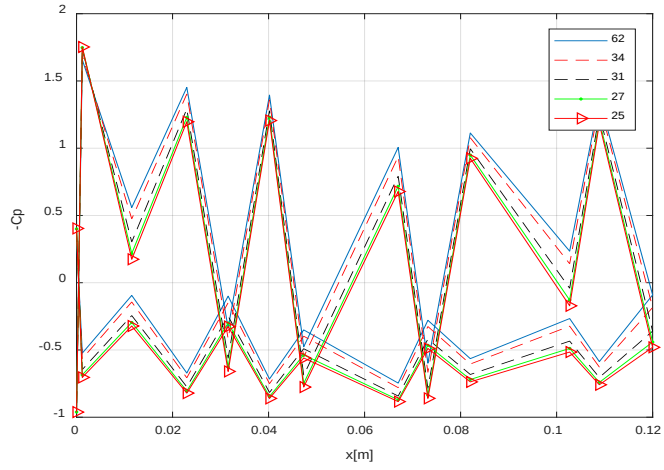

Figure 16. Effect of no of panels on Cp distribution of corrugated A airfoil for Re -19000 and 2^0 AOA

3.4 Validation of results

3.4.1 Corrugated A

The coefficient of lift for corrugated A airfoil at 2^0 angles of attack, was found similar by using the present panel method, experimental work and by Ho and New (2016). For $\alpha < 10^0$ panel method results showed an increase in the lift coefficient but for $\alpha > 10^0$, the results from Ho and New showed decrease in lift coefficient.

It must be noted that for three airfoils the drag coefficient was found nearly the same up to $\alpha < 8^0$. However, the panel method tends to predict higher drag coefficient by ~30 % as compared to experimental work as well from Ho and New, (2016). At higher angles of attack, $\alpha > 14^0$ all the three methods showed good agreement in results.

3.4.2 Corrugated B

For this airfoil, the lift coefficient prediction by Ho and New is lower as compared to present experimental and numerical work up to $\alpha \leq 12^0$. The present numerical results were in very close agreement with the present experimental work. Drag coefficient trends for corrugated B airfoil was nearly the same as corrugated A airfoil. At angle of attack of 14^0, the results by Ho and New (2016) showed higher value for the lift coefficient than the other two methods due to the flow separation that was observed in his work and due to the difference in the Reynolds number.

3.4.3 NACA 0010

The results for the glide ratio (C_L/C_D) of NACA 0010 airfoil obtained from the panel method were compared with experimental work from [20] and [24]. The Reynolds number was kept nearly the same during experiment (Re ~ 1.5 x 10^5) to ensure integrity in validation. The 2-D panel method predicted 25% higher values for the coefficient of lift at higher AOA ($\alpha > 10^0$) and lower drag at lower AOA for NACA 0010. The glide ratio trends for experimental and numerical methods also show nearly the same results. The C_L and C_D trends for numerical and experimental results are very close (< 5%) up to 8^0 AOA. Beyond this value the deviation in results is found to be high for the panel method to model the flow separation phenomenon. The corrugated B airfoil can be used to delay stall and the flow separation for higher angles of attack as the flow reattaches with the hump. The present study also revealed that basic panel methods are able to predict aerodynamic flow phenomenon fairly accurately for AOA ($\alpha < 8^0$). However, they are not suitable to analyze the unsteady effects and complex flow phenomenon like boundary layer flow separation and vortex shedding from either leading or trailing edge of the airfoil. The results also revealed that the lift coefficient for corrugated B airfoil was found higher as compared to remaining two airfoils. The drag coefficient for both corrugated A and B airfoils were found to be almost the same up to 12^0 AOA, whereas the glide ratio was found highest for corrugated A airfoil.

4. CONCLUSIONS

Basic panel method and experimental study were conducted to analyze the incompressible flow characteristics of NACA 0010 and two types of bio-inspired corrugated airfoils at chord Reynolds numbers 1.9×10^4 and 1.5×10^5. The present study revealed that the presence of corrugations on the wing surface improved the flow characteristics for low to moderate Reynolds numbers. The reason for the increased lift coefficient at higher angles of attack for corrugated airfoils is owing to formation of Leading edge vortices, which causes the large pressure difference between upper and lower surfaces which is not observed in conventional NACA airfoil. The panel method was able to predict the coefficient of lift and drag very well for lower angles of attack ($\alpha < 8^0$) and the results agreed well with computational work from Ho and New (2016). The presence of trailing edge hump on corrugated B airfoil increases the pressure coefficient at higher angles of attack which is similar to that observed near the trailing edge of NACA0010 airfoil.

REFERENCES

[1] J. D. Anderson, *Fundamentals of Aerodynamics, 5thEd*, McGraw Hills Inc, New York, 2012.

[2] C. Boller and C. M. Kuo, *Demonstration of adaptive structure performance on modular micro air vehicle*, Proceedings of 51st AIAA/ASME/ASCE/AHS/ASC structures, structural dynamics, and materials conference, Orlando, FL, USA, 2010.

[3] Y. H. Chen and M. Skote, Gliding performance of 3-D corrugated dragonfly wing with spanwise variation, *Journal of Fluid and Structures*, **62**: 1-13, doi: 10.1016/j.jfluidstructs 2015.

[4] T. Deubel, S. Wanke, C. Weber and F. Wedekind, *Modelling and manufacturing of a dragonfly wing as basis for bionic research*, Proceeding of 9th international design conference:215–220, Dubrovnik, 2006.

[5] H. Gao, H. Hu and Z. J. Wang, *Computational study of unsteady flows around dragonfly and smooth airfoils at low Reynolds numbers*, Proceedings of 46th AIAA aerospace sciences meeting and exhibit, Reno, NV, USA, 2008,doi.org/10.2514/6.2008-385, 2008.

[6] S. Gaurav and K. K. Jain, Numerical investigation of fluid flow and aerodynamic performance of a dragonfly wing section for micro air vehicles (MAVs) application, *Int. J. Innovat Scient Res*, **92**: 285–292, doi: 10.1.1.680.3222, 2014.

[7] W. H. Ho and T. H. New, Unsteady numerical investigation of two different corrugated airfoils, Proceedings of the Institution of Mechanical Engineers, *Part G: Journal of Aerospace Engineering*, Volume: **231** issue: 13, page(s): 2423-2437, doi: 10.1177/ 09544100 16682539, 2016.
[8] K. Hord and Y. S. Lian, Numerical investigation of the aerodynamic and structural characteristics of a corrugated airfoil, *Journal of Aircraft*, **49**(3): 749-757, doi.org/ 10.2514/ 1.C031135, 2012.
[9] E. L. Houghton and P. W. Carpenter, *Aerodynamics for engineering students*, 6th Ed. Butterworth-Heinemann Publication, Oxford, UK, 2013.
[10] H. Huand, M. Tamai, Bio-inspired corrugated airfoil at low Reynolds numbers, *J Aircraft*, **456**: 2068–2077, doi: 10.2514/1.37173, 2008
[11] A. B. Kesel, Aerodynamic characteristics of dragonfly wing sections compared with technical aerofoil, *J. Exp. Biol*., **203**: 3125–3135, doi.org/10.1016/S0010-4825 (98)018-3, 2000.
[12] A. B. Kesel, U. Philippi and W. Nachtigall, Biomechanical aspects of insect wing: an analysis using the finite element method, *Computers in Biology and Medicine*, **28**: 423-437, 1998.
[13] M. Kwok and R. Mittal, *Experimental investigation of the aerodynamics of a modelled dragonfly wing section*, Proceedings of AIAA Region-I MA Students Conference, https://doi.org/10.1155/2017/3019640, 2005.
[14] D. E. Levy and A. Seifert, Simplified dragonfly airfoil aerodynamics at Reynolds numbers below 8000, *Phys Fluids*, **21**: doi.org/10.1063, 2009.
[15] D. E. Levy and A. Seifert, Parameter study of simplified dragonfly airfoil geometry at Reynolds number of 6000, *J. TheoreticalBiology*, **266**(4):691–702, doi.org/10.1016/j.jtbi. 2010.07.016, 2010.
[16] T. Liu, K. Kuykendoll, R. Rhew, S. Jones, *Avian wings*, Proceeding 24th AIAA aerodynamic measurement technology and ground testing conference, Portland, OR, USA: 1–24, doi.org/10.2514/MAMT04, 2004.
[17] M. Mingallon and S. Ramaswamy, *The architecture of the dragonfly wing: A study of the structural and fluid dynamic capabilities of the Anisoptera's forewing*, Proceedings of the ASME 2011 international mechanical engineering congress & exposition: 1–8, New York, doi:10.1115/IMECE2011-62849, 2011.
[18] K. Muralidhar and T. T. Sundararajan, *Computational Fluid Flow and Heat Transfer*, 2nd Ed. Narosa Publishing House Ltd. New Delhi, India, 2011.
[19] J. Murphy and H. Hu, *An experimental investigation on a bio-inspired corrugated airfoil*, Proceedings of 47th AIAA aerospace sciences meeting and exhibit, Orlando, FL, USA, https://doi.org/10.2514/6.2009-1087, 2009.
[20] J. Murphy and H. Hu, An experimental study of a bio inspired corrugated airfoil for micro air vehicle applications, *Exp Fluids*, **492**: 531–546, doi:10.1007/s00348-010-0826-z., 2010.
[21] J. C. Nawrothet et. al, A tissue-engineered jellyfish with bio mimetic propulsion, *Nature, Biotechnology*, **30**(8): 792–797, doi: 10.1038/nbt.2269, 2012.
[22] T. H. New et al, Effects of corrugated aerofoil surface features on flow-separation control, *AIAA Journal* **521**:206–211, doi:10.1016, 2014.
[23] M. Okamoto, K. Yasuda and A. Azuma, Aerodynamic characteristics of the wings and body of a dragonfly, *J. Exp. Biology*, **199**: 281-294, 1996.
[24] B. N. Pamadi, *Performance, Stability, Dynamics, and Control of Airplanes*, Second Edition, AIAA. Inc Reston VA 20191-4344, 2004.
[25] C. J. C. Rees, Form and function in corrugated insect wings, *Nature***256**: 200–203. 1975a.
[26] C. J. C. Rees, Aerodynamic properties of an insect wing section and a smooth aerofoil compared, *Nature* **258**: 141–142, 1975b.
[27] S. X. Shi et al, *A*n experimental study of flow around a bio-inspired airfoil at Reynolds number $2.0x10^3$, *J Hydrodynamics*, **243**:410-419, doi.org/10.1016/S1001-6058(11)60262-X, 2010.
[28] A. Vargas and R. Mittal, *Aerodynamic Performance of Biological Airfoils*, Proceedings of 2nd Flow Control Conference, Portland, Oregon AIAA2004-2319, doi.org/10.2514/6.2004-2319, 2004.
[29] C. Webb, H. Dong and R. Mittal, *Motion kinematics effects on aerodynamic performance of bio-inspired wing sections inultra low Reynolds number flow*, Proceedings of 47th AIAA aerospace sciences meeting including the new horizons forum and aerospace exhibition, Orlando, FL, USA, doi.org/10.2514/6.2009-1300, 2009.
[30] J. H. Wu and M. Sun, Unsteady aerodynamic forces of a flapping wing, *J. Exp. Biology*, **207**:1137–1150, doi: 10.1242/jeb, 2004.